

Amino Acid-Functionalized Ionic Liquid Solid Sorbents for Post-Combustion Carbon Capture

Xianfeng Wang,^{†,‡} Novruz G. Akhmedov,[§] Yuhua Duan,[†] David Luebke,[†] David Hopkinson,[†] and Bingyun Li^{*,†,‡}

[†]National Energy Technology Laboratory-Regional University Alliance (NETL-RUA), Morgantown, West Virginia 26507, United States

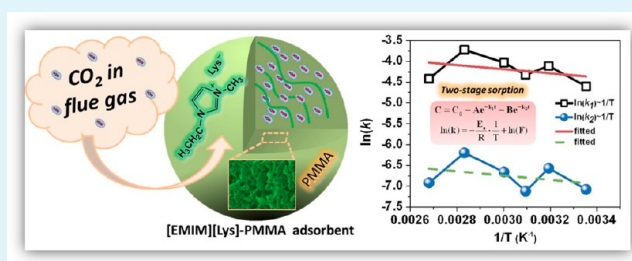
[‡]Department of Orthopaedics, School of Medicine, West Virginia University, Morgantown, West Virginia 26506, United States

[§]Department of Chemistry, West Virginia University, Morgantown, West Virginia 26506, United States

S Supporting Information

ABSTRACT: Amino acid ionic liquids (AAILs) are potential green substitutes of aqueous amine solutions for carbon dioxide (CO₂) capture. However, the viscous nature of AAILs greatly hinders their further development in CO₂ capture applications. In this contribution, 1-ethyl-3-methylimidazolium lysine ([EMIM][Lys]) was synthesized and immobilized into a porous poly(methyl methacrylate) (PMMA) microsphere support for post-combustion CO₂ capture. The [EMIM][Lys] exhibited good thermal stability and could be facilely immobilized into porous microspheres. Significantly, the [EMIM][Lys]-PMMA sorbents retained their porous structure after [EMIM][Lys] loading and exhibited fast kinetics. When exposed to CO₂ at 40 °C, [EMIM][Lys]-PMMA sorbent exhibited the highest CO₂ capacity compared to other counterparts studied and achieved a capacity of 0.87 mol/(mol AAIL) or 1.67 mmol/(g sorbent). The capture process may be characterized by two stages: CO₂ adsorption on the surface of sorbent and CO₂ diffusion into sorbent for further adsorption. The calculated activation energies of the two-stage CO₂ sorption were 4.1 and 4.3 kJ/mol, respectively, indicating that, overall, the CO₂ can easily adsorb onto this sorbent. Furthermore, multiple cycle tests indicated that the developed sorbents had good long-term stability. The developed sorbent may be a promising candidate for post-combustion CO₂ capture.

KEYWORDS: CO₂ capture, amino acid ionic liquid, activation energy, sorbent



1. INTRODUCTION

Global carbon dioxide (CO₂) emission caused by escalating energy use may have resulted in a series of environmental problems such as anomalous climate change and rising of sea levels.^{1–7} Studies have revealed that the concentration of CO₂ in the atmosphere has increased from a preindustrial value of ~280 ppm to the current 397 ppm, and this value is continuing to increase every year.^{8,9} In the United States, the combustion of carbon-based fossil fuels contributes over 94% to the anthropogenic CO₂ emission, and the U.S. Department of Energy (DOE) issued a carbon sequestration roadmap in 2009 aiming to achieve 90% CO₂ capture at an increased cost of electricity of no more than 35% for the post-combustion process by 2020.^{8,10,11} Carbon capture and storage (CCS) technology will be an effective approach to reducing excessive CO₂ emissions from fossil fuel combustion. One of the current leading technologies is the chemical absorption of CO₂ by aqueous amine solutions.^{12–15} However, this process is considered to be energy-intensive and expensive for large-scale CO₂ separation, as well as being corrosive and toxic in nature.^{16,17} Therefore, novel sorbent materials and technologies

for efficient and economical CO₂ capture have attracted increased attention in both academia and industry.

Ionic liquids (ILs) have been proposed as attractive alternatives for CO₂ capture because they have negligible volatility, nonflammability, high thermal stability, and virtually unlimited chemical tunability.^{18–20} Brennecke and co-workers first reported the solubility of CO₂ in imidazolium-based ILs under high pressures.²¹ The interaction between CO₂ and imidazolium-type ILs contributes to the activity of H-2 in the imidazolium ring. Because of the unique easily modified characteristics of ILs, alkaline groups (e.g., -NH₂) can be attached to ILs to act as a powerful functional group for CO₂ sorption.^{22,23} For example, Bates and co-workers introduced an amine group to the cation of ILs and reported that the CO₂ solubility of ILs increased substantially.²² Since then, a number of amine-functionalized ILs have been developed for CO₂ capture.^{24–26} Amino acids (AAs) were one type that have been used as both anions and cations to prepare novel ILs.^{27–29}

Received: June 13, 2013

Accepted: August 8, 2013

Published: August 8, 2013

In 2005, Fukumoto et al.²⁸ first reported the preparation of amino acid-based ILs (AAILs) from 20 natural AAs by a neutralization method. In general, NH_3^+ in AAILs could be deprotonated and result in an active $-\text{NH}_2$ group for CO_2 sorption.

Although the CO_2 absorption in AAILs was substantially improved, their use as liquid solvents is still limited due to their viscous nature. For instance, AAILs containing tetrabutylphosphonium as a cation were found to have a minimum viscosity of 344 mPa s at 25 °C,³⁰ and most AAILs that were prepared using AAs as cations or using AA derivatives were either solids or liquids of extremely high viscosity, up to 4180 mPa s at room temperature.³¹ In order to reduce the viscosity of AAILs, Jiang et al.²⁰ successfully synthesized low viscosity (<60 mPa s) AAILs using symmetric tetraalkylammonium ([TAA]) as a cation; however, the resulting CO_2 capacity of 0.32 mol/(mol AAIL) was not ideal for large-scale CO_2 removal. Immobilization of AAILs into porous supports may enhance the CO_2 sorption rate and keep the high CO_2 capacity of AAILs themselves, which is regarded as a promising strategy to synthesize advanced sorbents for CO_2 removal.^{29,32,33}

Herein, 1-ethyl-3-methylimidazolium ILs with lysine as a reactive AA anion ([EMIM][Lys]) was synthesized and further immobilized into porous polymethylmethacrylate (PMMA) microspheres through a facile wet impregnation–vaporization method. Lys was selected because of its high content of the amino groups and thus high capacity potential.¹⁸ The resulting sorbents were characterized, and their CO_2 capture properties were investigated. On the basis of our previous pilot work on AAIL-based solid sorbents,³³ this study aimed at generating AAIL sorbents with high sorption rate, high capacity, and excellent long-term stability, as well as examining the capture mechanism and related activation energy. The developed AAIL-based solid sorbents were characterized, and their CO_2 capture properties were investigated. The sorbents exhibited a high sorption rate and capacity, good recyclability, and high thermal and long-term stability.

2. EXPERIMENTAL SECTION

2.1. Materials. 1-Ethyl-3-methylimidazolium bromide ([EMIM][Br], ≥97.0%), Lys, glycine (Gly), alanine (Ala), arginine (Arg), anion exchange resin (Amberlite IRA400 hydroxide), and ethanol were purchased from Sigma Aldrich Co. (St. Louis, MO). Figure S1 of the Supporting Information shows the structure of [EMIM][Br] and AAs selected for this study. PMMA microparticles (effective particle size ~0.5 μm and specific surface area 547 m²/g) were purchased from Supelco Co. (Bellefonte, PA). CO_2 and N_2 of high purity were used for thermogravimetric analysis (TGA).

2.2. Synthesis of [EMIM][AA]. [EMIM][Lys] was synthesized via a neutralization method.^{28,33} A total of 1.0 g of [EMIM][Br] was dissolved in deionized water (20 mL) to prepare an aqueous solution and passed through the anion exchange resin, Amberlite IRA400 (OH-type), to prepare the [EMIM][OH] solution. Then, the [EMIM][OH] solution was reacted with a slight excess of Lys (0.9 g) through neutralization at room temperature for 24 h. Water was evaporated to generate a residual solution that contained the required IL. After being further dried at 50 °C under vacuum for 12 h, the residue was diluted with ethanol (8 mL) to precipitate the excess Lys. After centrifuging at 3750 rpm for 15 min, the insoluble Lys was removed and the ethanol in the resultant solution was removed by rotating evaporation. Finally, the products were dried at 80 °C under vacuum for 12 h before being used for further characterization and immobilization. In order to determine the effect of AA anion on the performance of the sorbents, three other AAILs (i.e., [EMIM][Gly], [EMIM][Ala], [EMIM][Arg]) were synthesized in a similar fashion.

2.3. Preparation of [EMIM][AA]-impregnated PMMA Sorbents. [EMIM][AA]-impregnated PMMA sorbents were synthesized through a well-studied wet impregnation–vaporization method.^{18,33–37} Briefly, [EMIM][AA] was dissolved in ethanol at a concentration of 50 mg/mL under a rotary evaporator (RV 10 Basic Plus D, Wilmington, NC) using a stirring rate of 100 rpm. After 30 min, PMMA microparticles were added. The suspension was continuously stirred for about 2 h under vacuum and subsequently dried at 50 °C for 6 h. [EMIM][AA]–PMMA sorbents with various loadings (i.e., 37.5, 48.7, and 58.5 wt %) of immobilized [EMIM][AA] were prepared. The amount of AAILs loaded in the PMMA microparticles was determined by comparing the weight differences of the PMMA particles used before and after impregnation.

2.4. Characterization. The ¹H nuclear magnetic resonance (NMR) spectrum of [EMIM][Lys] was recorded at 25 °C using a Varian INOVA 600 MHz spectrometer equipped with a triple-resonance z-axis pulsed field gradient 5 mm probe. TGA and differential scanning calorimetry (DSC) of [EMIM][Lys] were performed on an SDT Q600 (V20.9 Build 20) instrument (Artisan Technology Group, Champaign, IL) under N_2 atmosphere with a heating rate of 10 °C/min. The morphology of PMMA microparticles was examined using scanning electron microscopy (SEM) (Hitachi S-4700, Tokyo, Japan). PMMA microparticles were cut into half using a thin sharp blade under an optical microscope. Samples were mounted onto stainless steel supports and sputtered with gold, and the sample cross sections were examined. Brunauer–Emmett–Teller (BET) and Barrett–Joyner–Halenda (BJH) analyses of resultant sorbents were examined by the nitrogen adsorption/desorption test with the help of a surface area analyzer (ASAP 2020).

2.5. CO_2 Capture and Regeneration of AAIL Sorbents. The CO_2 capture performance of [EMIM][AA]-impregnated PMMA sorbents was determined using TGA. Thirty milligrams of dried PMMA-based sorbent was placed into the middle of the TGA microbalance quartz tube reactor and heated to 105 °C in a N_2 atmosphere at a flow of 200 mL/min for about 60 min. The temperature was then adjusted to 40 °C (or 25, 50, 60, 80, 100 °C for determining the effect of temperature on CO_2 capture performance), and pure dry CO_2 was introduced at a gas flow rate of 200 mL/min until no obvious weight gain was observed. The desorption was performed by introducing pure N_2 into the sample cell at 100 °C for 60 min. The weight change in milligrams of the sorbents was recorded, and the weight change in percentage was defined as the ratio of the amount of the gas adsorbed or desorbed over the total amount of CO_2 adsorbed. Adsorption capacity in mmol/(g sorbent) was calculated from the weight change of the samples during the adsorption/desorption cycles. To check the stability of the sorbents, after the first sorption cycle, the cycling was repeated by heating the sorbents to 100 °C under N_2 for regeneration, followed by cooling to 40 °C for another CO_2 adsorption process.

3. RESULTS AND DISCUSSION

[EMIM][Lys] and other three AAILs (i.e., [EMIM][Gly], [EMIM][Ala], [EMIM][Arg]) were transparent light yellow liquids at room temperature (Figure S2, Supporting Information). The structure of [EMIM][Lys] was confirmed using ¹H NMR spectroscopy (Figure S3, Supporting Information). Figure 1 shows the TGA and DSC curves of as-prepared [EMIM][Lys]. It can be seen that [EMIM][Lys] had an onset thermal decomposition temperature (T_d) of about 200 °C, indicating reasonably good thermal stability. For the DSC test (Figure 1), an exothermic peak was observed around 200 °C for [EMIM][Lys], which may be associated with the curing process (i.e., cold crystallization) of [EMIM][Lys].^{38,39} The cold crystallization temperature is the onset of an exothermic peak on heating from a subcooled liquid state to a crystalline solid state, which has been observed previously for ILs.³⁸ An endothermic effect was observed around 250 °C, which may be related to the thermal degradation of [EMIM][Lys] in N_2 .

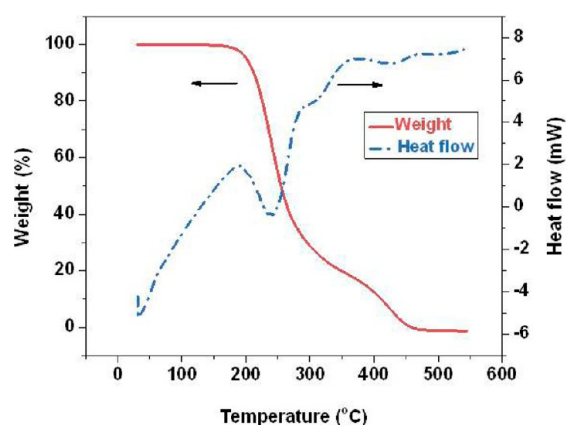


Figure 1. TGA and DSC curves of as-prepared [EMIM][Lys] (N_2 atmosphere, heating rate of $10\text{ }^\circ\text{C}/\text{min}$).

Figure 2 shows the CO_2 uptake behavior of the [EMIM]-[Lys] solvent with different amounts of the sample placed in

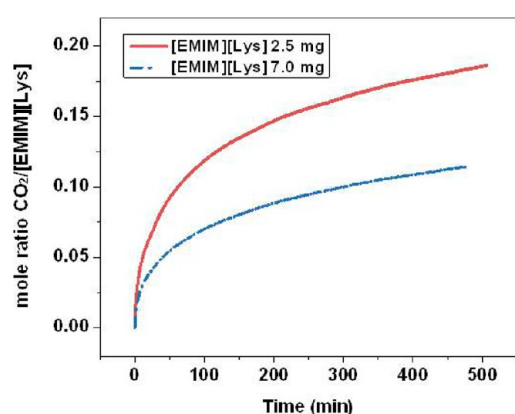


Figure 2. CO_2 absorption of [EMIM][Lys] solvents with different amount placed in the TGA sample cell at $40\text{ }^\circ\text{C}$.

the TGA microbalance quartz sample cell. The liquid [EMIM][Lys] was heated to $105\text{ }^\circ\text{C}$ in a N_2 atmosphere to remove moisture and then adjusted to $40\text{ }^\circ\text{C}$ in CO_2 to measure CO_2 capacity. The sorption rate of liquid [EMIM]-[Lys] was slower at 7 mg of sample size compared to 2.5 mg. This finding could be attributed to the high CO_2 diffusion resistance caused by the high viscosity of the AAILs. For the 7 mg sample, the molar uptake of CO_2 per mole of [EMIM][Lys] during 500 min exposure period was approximately 0.12. When the amount of [EMIM][Lys] was reduced to 2.5 mg, the sample could be effectively spread as a thin film in the sample cell, and the sorption rate was enhanced, reaching a sorption capacity of 0.19 mol/(mol [EMIM][Lys]) in 500 min. However, this experimental CO_2 absorption capacity was still much lower than the theoretical value, possibly due to the high viscosity of the imidazolium-based AAIL caused by the hydrogen bonding at the 2-position of the imidazolium cation ring with its AA anions.^{20,28}

In order to improve the absorption performance, [EMIM]-[Lys] was immobilized into nanoporous PMMA microparticles using an impregnation–vaporization method. Here, PMMA microparticles were selected as a standard support because of their hierarchical structure and large BET surface area ($547\text{ m}^2/\text{g}$), which could be beneficial for the increase in AAIL loading and CO_2 diffusion.^{40,41} Figure 3 shows the SEM images of the

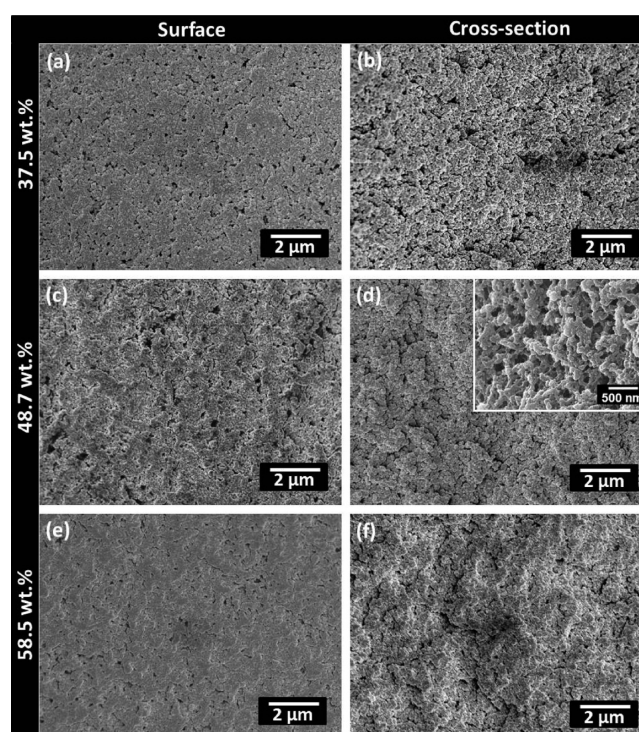


Figure 3. SEM images of as-prepared [EMIM][Lys]–PMMA sorbents with different [EMIM][Lys] loadings (37.5, 48.7, and 58.5 wt %). Left: Surface structures; Right: Cross-section structures.

as-prepared [EMIM][Lys]–PMMA sorbents with different amounts of [EMIM][Lys] loaded (37.5, 48.7, and 58.5 wt %), indicating that the surfaces of the PMMA microspheres are featured with hierarchical roughness and nanotextures. Close observation of the cross-section of the sorbents with [EMIM]-[Lys] loading of 48.7 wt % (Figure 3d, inset) showed that the microspheres retained their interior porous structure after immobilization of [EMIM][Lys]. These observations lead us to the conclusion that the nanoporous structure of the developed sorbents may be suitable for mass (e.g., CO_2) transport and have potential for CO_2 capture applications.

The N_2 adsorption/desorption isotherms of PMMA microparticles before and after loading [EMIM][Lys] were measured to evaluate their surface area and pore structure. As shown in Figure 4 and Table S1 of the Supporting Information, the original PMMA microparticles exhibited very high N_2 uptakes with a saturated uptake of $958\text{ cm}^3/\text{g}$. The corresponding BET surface area and BJH adsorption cumulative pore volume were calculated to be $547\text{ m}^2/\text{g}$ and $1.34\text{ cm}^3/\text{g}$, respectively. After [EMIM][Lys] was loaded into PMMA microparticles, the N_2 uptake, surface area and pore volume decreased dramatically. As shown in Figure 4 and Table S1 of the Supporting Information, the saturated N_2 uptake ($333\text{ cm}^3/\text{g}$) and pore volume ($0.50\text{ cm}^3/\text{g}$) of [EMIM][Lys](37.5 wt %)-PMMA were roughly one-third of those of PMMA microparticles. The BET surface area was reduced to $94\text{ m}^2/\text{g}$. Particularly, the reduced pore volume confirmed that the [EMIM][Lys] was loaded into PMMA pores. Comparison between reduced pore volume from N_2 adsorption analysis and loaded AAIL volume (Table S2, Supporting Information) further confirmed that some pores of the sorbents were blocked by AAIL loading. When the [EMIM][Lys] loading was increased to 48.7 wt %, the saturated N_2 uptake, BET surface area, and pore volume

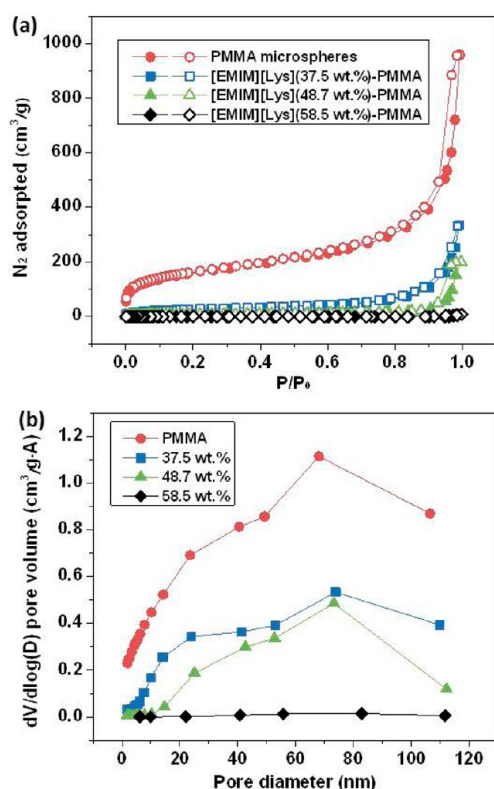


Figure 4. (a) N₂ adsorption/desorption isotherms and (b) BJH adsorption pore size distribution of PMMA microspheres before and after loading [EMIM][Lys]. The filled symbols are for adsorption and empty symbols for desorption.

were drastically dropped to 200 cm³/g, 27 m²/g, and 0.31 cm³/g, respectively. When the loading of [EMIM][Lys] was further increased to 58.5 wt %, the resulting BET surface area and pore volume were only 0.77 m²/g and 0.01 cm³/g, respectively, indicating the almost complete pore filling/blockage of PMMA microparticles by [EMIM][Lys] (Figure 3e and f). BJH adsorption pore size distribution (Figure 4b) presented the changes of pore sizes with increasing [EMIM][Lys] loading, suggested that the majority of the pores were smaller than 120 nm.

Figure 5 presents the CO₂ capture performance of [EMIM][Lys]–PMMA sorbent with various [EMIM][Lys]

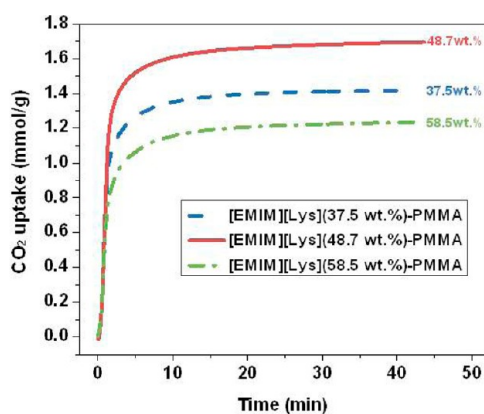


Figure 5. CO₂ adsorption of [EMIM][Lys]–PMMA sorbents with various [EMIM][Lys] weight ratios (i.e., 37.5, 48.7, and 58.5 wt %) in the sorbents at 40 °C.

weight ratios in the sorbents at 40 °C. It demonstrated that the resultant sorbents can overcome the high viscosities of [EMIM][Lys] to exhibit a dramatically enhanced sorption rate (reaching their equilibrium sorption capacity within 10 min) and capacity [(1.23–1.67 mmol/(g sorbent) or 0.64–0.87 mol/(mol [EMIM][Lys])], which could be due to the enlarged mass transfer area of AAILs after immobilization.¹⁸ Evidently, the CO₂ adsorption capacity of our [EMIM][Lys]–based sorbents was also much higher than [TAA][AA] with a low viscosity, which had a capacity of 0.32 mol/(mol AAIL).²⁰ Amine-based ILs are known to react with CO₂ to produce carbamates through the formation of zwitterionic intermediates.⁴² Additionally, the CO₂ capture behaviors depend on the [EMIM][Lys] weight ratios in the sorbents. The CO₂ adsorption capacity of [EMIM][Lys]–PMMA with [EMIM][Lys] loadings of 37.5, 48.7, 58.5 wt % were 1.42, 1.67, 1.23 mmol/(g sorbent), respectively (Figure 5). The CO₂ adsorption capacity increased with increasing [EMIM][Lys] loading from 37.5 to 48.7 wt % followed by a decrease at 58.5 wt % loading. The capacity reached the highest level of 1.67 mmol/(g sorbent) or 0.87 mol/(mol AAIL) at the [EMIM][Lys] loading of 48.7 wt %; a CO₂ adsorption capacity of >1 mmol/(g sorbent) was indicated to potentially reduce the cost of CO₂ sequestration.⁴³ At 48.7 wt % loading of [EMIM][Lys], appreciable porosity was still preserved (Figure 4) with similar pore sizes inside and outside the porous PMMA support (Figure 3c and d), and this was beneficial for CO₂ adsorption and led to high amine efficiency. Upon further increasing the loading of [EMIM][Lys] to 58.5 wt %, the large amount of [EMIM][Lys] could have blocked the pores of PMMA particles (Figure 3e and f) and thus reduced the specific surface area (0.77 m²/g) and pore volume (0.01 cm³/g) of the sorbents (Table S1, Supporting Information and Figure 4b) leading to a lower capacity [1.23 mmol/(g sorbent)].

It is known that CO₂ sorption by supported amine sorbents is temperature dependent.⁴⁴ The [EMIM][Lys](48.7 wt %)-PMMA sorbent was exposed to CO₂ at a temperature range from 25 to 100 °C. Clearly, as the temperature increased, the CO₂ capture capacity decreased (Figure 6a). A plot of CO₂ capacity versus temperature (Figure 6b) shows that there was a trend toward linear decrease, and the CO₂ uptake amount reached the highest [1.87 mmol/(g sorbent)] and lowest [1.47 mmol/(g sorbent)] levels at sorption temperature of 25 and 100 °C, respectively. This phenomenon occurs because the interaction between a sorbent and a sorbate was weakened as temperature increases.⁴⁵ In general, the adsorption process can be described well with a single or a series of multiple first-order reactions.^{46,47} Hence, the adsorption curves in Figure 6a are fitted into the following double exponential model:

$$C = C_0 - Ae^{-k_1 t} - Be^{-k_2 t} \quad (1)$$

where k_1 and k_2 are the reaction rate constants, t is the time, A and B are parameters, and C_0 is the saturated capacity. The results are shown in Figure S4 of the Supporting Information, and the fitted parameters are listed in Table 1. The adsorption curves were also fitted using other models, e.g., a single exponential model (Figure S5, Supporting Information).

From Figures S4 and S5 of the Supporting Information, one can see that these adsorption curves fit very well in a double exponential model (Figure S4, Supporting Information) as compared to a single exponential model (Figure S5, Supporting Information). These results indicated that CO₂ adsorption in [EMIM][Lys]–PMMA sorbents may have two different

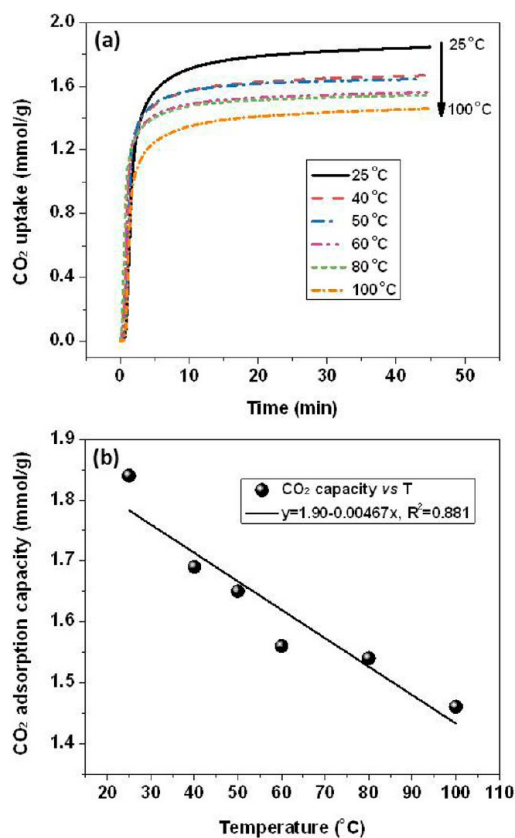


Figure 6. (a) CO₂ adsorption of [EMIM][Lys](48.7 wt %)-PMMA sorbent at 25, 40, 50, 60, 80, and 100 °C. (b) CO₂ capacity vs temperature.

sorption processes: (1) CO₂ adsorption on the surface (k_1), where the CO₂ directly reacts with the surface amino group to form carbamate, which was a fast process. (2) Once the surface amino groups bonded with CO₂, the CO₂ has to diffuse into the sorbent to continue reacting with amino groups. Obviously, this was a kinetically controlled step (k_2) as we can see from Table 1; k_1 was at least an order of magnitude higher than k_2 . From Table 1, we also found that with increasing temperature from 25 to 80 °C, k_1 and k_2 increased overall. However, when the temperature reached 100 °C, k_1 and k_2 decreased. As shown in Figure 6 and Table 1, as temperature increased, the CO₂ capacity decreased and the reaction time to reach the maximum capacity did not change much. Therefore, this sorbent was more suitable for low-temperature (<80 °C) CO₂ capture technology.

For each sorption process, the activation energy can be obtained by applying the following Arrhenius equation.⁴⁷

$$\ln(k) = -\frac{E_a}{R} \times \frac{1}{T} + \ln(F) \quad (2)$$

Table 1. Fitted CO₂ Capture Kinetic Parameters of [EMIM][Lys](48.7 wt %)-PMMA Sorbent

T (K)	k_1 (sec ⁻¹)	k_2 (sec ⁻¹)	A (mmol/g)	B (mmol/g)	C ₀ (mmol/g)	R ²
298.15	1.0067×10^{-2}	8.4491×10^{-4}	2.0533	0.2438	1.8706	0.9781
313.15	1.6432×10^{-2}	1.4058×10^{-3}	1.7264	0.2398	1.6704	0.9857
323.15	1.3261×10^{-2}	8.1013×10^{-4}	1.9609	0.1409	1.6643	0.9642
333.15	1.7797×10^{-2}	1.2835×10^{-3}	1.7562	0.1775	1.5649	0.9768
353.15	2.4251×10^{-2}	2.0339×10^{-3}	1.5613	0.2418	1.5379	0.9891
373.15	1.2089×10^{-2}	9.9098×10^{-4}	1.6168	0.2169	1.4725	0.9732

where k is the reaction rate constant, R is the gas constant, E_a is the activation energy, and F is the pre-factor. By plotting $\ln(k)$ versus $1/T$ (Figure 7), we obtained the activation energies of

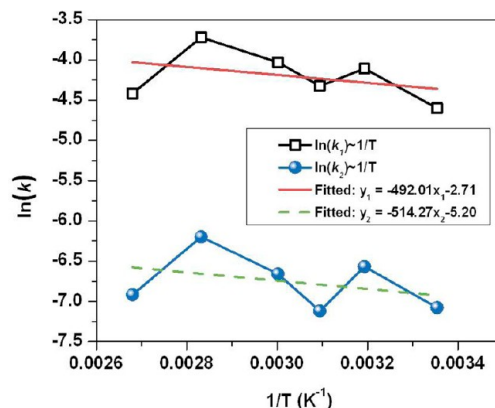


Figure 7. The $\ln(k) \sim 1/T$ relationship from the Arrhenius' equation.

Table 2. Fitted Activation Energy (E_a) and Pre-Factor F of [EMIM][Lys](48.7 wt %)-PMMA Sorbent

	E_a (kJ/mol)	F
1st process	4.1	6.65×10^{-2}
2nd process	4.3	6.32×10^{-6}

these two sorption processes (Table 2). Although there are large deviations from linearity (especially the data at 100 °C) in Figure 7, it was surprising to see that the activation energies for both processes were similar, which may indicate that the activation barrier was not the main reason for the rate differences (Table 1). As we know, the pre-factor (F in eq 2) was related to the entropy change of the sorption system. Compared to the first process, the second process of CO₂ diffusion had a lower pre-factor value (Table 2), which corresponded to less entropy change. Therefore, although their activation energies were similar, the first process had a larger entropy change and a larger reaction rate constant, while the second process was the rate determining step with smaller reaction rate constant and entropy change.

In addition to the high CO₂ capture efficiency, long-term stability is also important for any CO₂ sequestration system.⁴⁴ Figure 8 presents the CO₂ adsorption/desorption multicycles of [EMIM][Lys]-PMMA (48.7 wt %) sorbent. It can be seen that the sorbents can be used in many cycles, maintaining nearly constant adsorption capacity. Only a 4% loss in adsorption capacity was observed after 14 cycles for [EMIM][Lys]-PMMA (48.7 wt %) sorbent. The high stability of [EMIM][Lys]-PMMA sorbent may be attributed to its lower

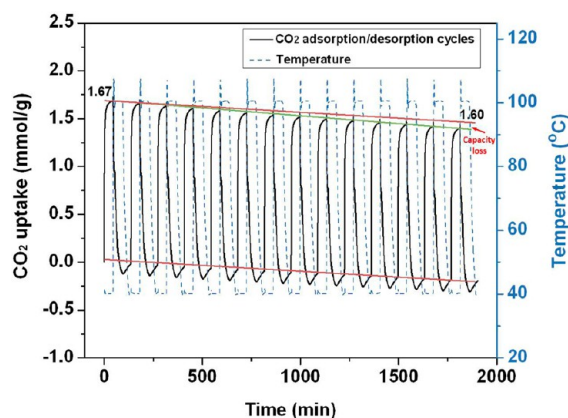


Figure 8. (a) CO₂ adsorption vs cycles of [EMIM][Lys] (48.7 wt %)–PMMA sorbent. Each cycle consisted of flowing CO₂ at 40 °C for 45 min and then flowing N₂ at 100 °C for 45 min.

volatility and solid state at room temperature. It suggests that the slight loss of sorption capacity may result from weight loss of the immobilized AAIL during the temperature- and pressure-swung regeneration process.⁴⁸ For wet-impregnated solid amine sorbents (e.g., AAIL-based sorbents), the amine molecules adhere to the porous support surface by physical van der Waals forces or hydrogen bonding and may leak to the bulk gas stream because of the difference in concentration, which contributes to the loss of amines.⁴⁹

To determine the effect of AA anion on CO₂ capture performance of the sorbents, different AA (i.e., Lys, Gly, Ala, Arg)-based [EMIM][AA]s with similar loading were immobilized into PMMA microparticles, and their CO₂ uptake performance was determined using the TGA method (Figure 9); the results are summarized in Table 3. Note that all the sorbents were tested under ideal conditions (i.e., dry, pure gas, with a CO₂ partial pressure of 1 bar, and desorbing with N₂); this simple adsorption/desorption test was useful in comparing the performance of different types of sorbents. All the sorbents exhibited a rapid initial sorption rate and high capacity [1.01–1.67 mmol/(g sorbent) or 0.45–0.87 mol/(mol AAIL)] (Figure 9a). The CO₂ capture behaviors depended on the AA anion. When exposed to CO₂, the adsorption capacity of [EMIM][Arg], [EMIM][Ala], [EMIM][Gly], and [EMIM][Lys] were 1.01, 1.38, 1.53, and 1.67 mmol/(g sorbent), respectively (Figure 9b). Evidently, the [EMIM][Lys]-based sorbent achieved the best CO₂ capture performance in 50 min (87% of its theoretical value), which could be attributed to its high content of amino groups (i.e., two amino groups in one molecule). Note that the capacity could be further improved by choosing better porous supports, which will be part of our future studies. It is known that aqueous amine absorbs CO₂ in a 1:2 stoichiometry (i.e., one CO₂ molecule is combined with two amino groups).²² For amino-functionalized task-specific ILs, both 1:1 and 1:2 reaction stoichiometry mechanisms have been proposed.^{18,22} In this work, the adsorption mechanism of CO₂ in developed [EMIM][AA]–PMMA sorbents was believed to follow the 1:2 stoichiometry (except [EMIM][Arg]). According to the 1:2 stoichiometry, at most, 0.5–1.5 mol CO₂ can be sorbed per mol [EMIM][AA] based on the number of sites for CO₂ bonding. The experimental CO₂ sorption capacities of sorbents approached their theoretical maximum value (Table 3). The experimental CO₂ sorption capacity of [EMIM][Arg] presented an obvious discrepancy

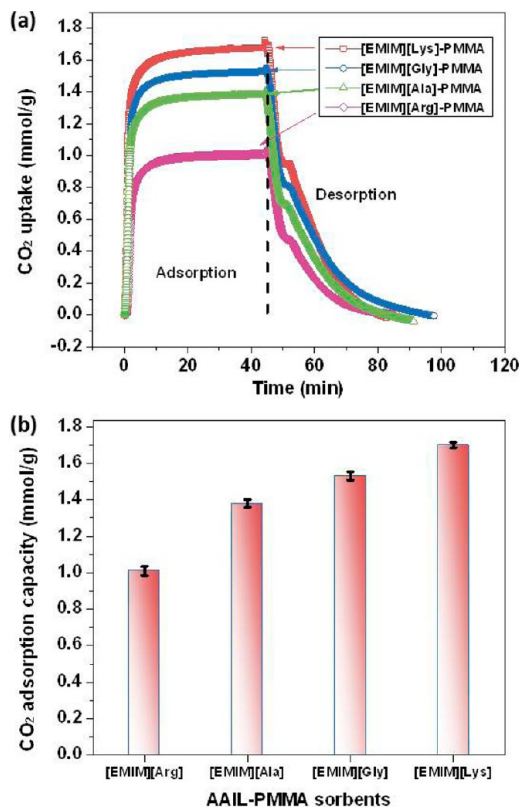


Figure 9. (a) CO₂ adsorption/desorption curves and (b) CO₂ adsorption capacity of four different [EMIM][AA]–PMMA sorbents (with [EMIM][AA] weight ratio of ~48.7 wt % in the sorbents).

with its theoretical one, which could be related to the possible formation of hydrogen bonds among the Arg molecules thereby rendering them inactive for CO₂ sorption.^{18,24}

4. CONCLUSIONS

AA-functionalized [EMIM]-type AAILs were synthesized and immobilized into nanoporous PMMA microspheres as new sorbents for post-combustion CO₂ removal. The [EMIM][Lys] exhibited good thermal stability and could be facilely immobilized into nanoporous microparticles with various weight ratios. After [EMIM][Lys] loading, the nanoporous structure of PMMA particles was retained, and [EMIM][Lys] was well distributed onto/into the surface/interior of the porous support, leading to fast kinetics of [EMIM][Lys]–PMMA sorbent. Compared with the other three AAILs studied (i.e., [EMIM][Arg], [EMIM][Ala], [EMIM][Gly]), [EMIM][Lys]–PMMA sorbent had the highest CO₂ capture capacity [1.67 mmol/(g sorbent) or 0.87 mol/(mol AAIL)]. The CO₂ adsorption in AAIL sorbents seemed to involve two processes: CO₂ was directly adsorbed on the surface and CO₂ diffused into the sorbent to continue reacting with amino groups. Our fitted rate constants, activation energies, and pre-factors (related to entropy change) showed that the second process for CO₂ diffusion was the rate-determining step for the sorbent to capture CO₂. The CO₂ uptake performance of the [EMIM][Lys]–PMMA sorbent could be finely controlled by adjusting the sorbent structure, AAIL loading, sorption temperature, and gas flow rate. Furthermore, the developed [EMIM][Lys]–PMMA sorbent had stable multi-cyclic properties and may be promising for post-combustion CO₂ capture.

Table 3. CO₂ Sorption Capacity (C) of the Four Sorbents with [EMIM][AA] Loading of ~48.7 wt %

sample	C _{theo} (mol/mol) ^a	C _{exp} (mol/mol) ^b	C _{exp} [mmol/(g IL)]	C _{exp} [mmol/(g sorbent)]
[EMIM][Lys]–PMMA	1	0.87	3.40	1.67
[EMIM][Gly]–PMMA	0.5	0.49	3.06	1.53
[EMIM][Ala]–PMMA	0.5	0.45	2.76	1.38
[EMIM][Arg]–PMMA	1.5	0.52	2.02	1.01

^aTheoretical CO₂ sorption capacity. ^bExperimental CO₂ sorption capacity.

■ ASSOCIATED CONTENT

📄 Supporting Information

Chemical structure of [EMIM][Br] and amino acids, optical images of prepared AAILs, ¹H NMR spectrum of [EMIM]-[Lys], fitted curves for CO₂ adsorption using single and double exponential models, N₂ adsorption/desorption analyses of sorbents, and comparison between loaded [EMIM][Lys] volume and reduced pore volume from BJH adsorption analysis. This material is available free of charge via the Internet at <http://pubs.acs.org>.

■ AUTHOR INFORMATION

Corresponding Author

*Tel: +1-304-293-1075. Fax: +1-304-293-7070. E-mail: bili@hsc.wvu.edu. URL: <http://www.hsc.wvu.edu/som/ortho/bli/>.

Notes

The authors declare no competing financial interest.

■ ACKNOWLEDGMENTS

As part of the National Energy Technology Laboratory's Regional University Alliance (NETL-RUA), a collaborative initiative of the NETL, this technical effort was performed under RES contract DE-FE0004000. Support was also received from WV NASA EPSCoR. Any opinions, findings, conclusions, or recommendations expressed in this material are those of the author(s) and do not necessarily reflect the views of the funding agencies or their institutions. The authors thank Bryan Morreale, George A. Richards, and Henry W. Pennline for their support and Suzanne Danley for proofreading.

■ REFERENCES

- Du, N.; Park, H. B.; Dal-Cin, M. M.; Guiver, M. D. *Energy Environ. Sci.* **2012**, *5*, 7306–7322.
- Xing, W.; Liu, C.; Zhou, Z.; Zhang, L.; Zhou, J.; Zhuo, S.; Yan, Z.; Gao, H.; Wang, G.; Qiao, S. Z. *Energy Environ. Sci.* **2012**, *5*, 7323–7327.
- Banerjee, R.; Phan, A.; Wang, B.; Knobler, C.; Furukawa, H.; O'Keeffe, M.; Yaghi, O. M. *Science* **2008**, *319*, 939–943.
- Duan, Y. H.; Luebke, D. R.; Pennline, H. W.; Li, B. Y.; Janik, M. J.; Halley, J. W. *J. Phys. Chem. C* **2012**, *116*, 14461–14470.
- Tanthana, J.; Chuang, S. S. C. *ChemSusChem* **2010**, *3*, 957–964.
- Jeon, H. J.; Choi, J. H.; Lee, Y.; Choi, K. M.; Park, J. H.; Kang, J. K. *Adv. Energy Mater.* **2012**, *2*, 225–228.
- Qian, D.; Lei, C.; Hao, G. P.; Li, W. C.; Lu, A. H. *ACS Appl. Mater. Interfaces* **2012**, *4*, 6125–6132.
- Liu, J.; Thallapally, P. K.; McGrail, B. P.; Brown, D. R. *Chem. Soc. Rev.* **2012**, *41*, 2308–2322.
- Wang, J. C.; Senkowska, I.; Oschatz, M.; Lohe, M. R.; Borchardt, L.; Heerwig, A.; Liu, Q.; Kaskel, S. *ACS Appl. Mater. Interfaces* **2013**, *5*, 3160–3167.
- Ciferno, J. P.; Fout, T. E.; Jones, A. P.; Murphy, J. T. *Chem. Eng. Prog.* **2009**, *105*, 33–41.
- Stauffer, P. H.; Keating, G. N.; Middleton, R. S.; Viswanathan, H. S.; Berchtold, K. A.; Singh, R. P.; Pawar, R. J.; Mancino, A. *Environ. Sci. Technol.* **2011**, *45*, 8597–8604.
- Ma, X. L.; Wang, X. X.; Song, C. S. *J. Am. Chem. Soc.* **2009**, *131*, 5777–5783.
- Wang, X. X.; Schwartz, V.; Clark, J. C.; Ma, X. L.; Overbury, S. H.; Xu, X. C.; Song, C. S. *J. Phys. Chem. C* **2009**, *113*, 7260–7268.
- Li, B.; Duan, Y.; Luebke, D.; Morreale, B. *Appl. Energy* **2013**, *102*, 1439–1447.
- Rezaei, F.; Lively, R. P.; Labreche, Y.; Chen, G.; Fan, Y.; Koros, W. J.; Jones, C. W. *ACS Appl. Mater. Interfaces* **2013**, *5*, 3921–3931.
- Zhang, S. H.; Lu, Y. Q.; Ye, X. H. *Int. J. Greenhouse Gas Control* **2013**, *13*, 17–25.
- Srikanth, C. S.; Chuang, S. S. C. *ChemSusChem* **2012**, *5*, 1435–1442.
- Ren, J.; Wu, L. B.; Li, B. G. *Ind. Eng. Chem. Res.* **2012**, *51*, 7901–7909.
- Gurkan, B. E.; de la Fuente, J. C.; Mindrup, E. M.; Ficke, L. E.; Goodrich, B. F.; Price, E. A.; Schneider, W. F.; Brennecke, J. F. *J. Am. Chem. Soc.* **2010**, *132*, 2116–2117.
- Jiang, Y. Y.; Wang, G. N.; Zhou, Z.; Wu, Y. T.; Geng, J.; Zhang, Z. B. *Chem. Commun.* **2008**, *4*, 505–507.
- Anthony, J. L.; Maginn, E. J.; Brennecke, J. F. *J. Phys. Chem. B* **2002**, *106*, 7315–7320.
- Bates, E. D.; Mayton, R. D.; Ntai, I.; Davis, J. H. *J. Am. Chem. Soc.* **2002**, *124*, 926–927.
- Brennecke, J. E.; Gurkan, B. E. *J. Phys. Chem. Lett* **2010**, *1*, 3459–3464.
- Goodrich, B. F.; de la Fuente, J. C.; Gurkan, B. E.; Zadijian, D. J.; Price, E. A.; Huang, Y.; Brennecke, J. F. *Ind. Eng. Chem. Res.* **2010**, *50*, 111–118.
- Goodrich, B. F.; de la Fuente, J. C.; Gurkan, B. E.; Lopez, Z. K.; Price, E. A.; Huang, Y.; Brennecke, J. F. *J. Phys. Chem. B* **2011**, *115*, 9140–9150.
- Gutowski, K. E.; Maginn, E. J. *J. Am. Chem. Soc.* **2008**, *130*, 14690–14704.
- Tao, G. H.; He, L.; Sun, N.; Kou, Y. *Chem. Commun.* **2005**, *28*, 3562–3564.
- Fukumoto, K.; Yoshizawa, M.; Ohno, H. *J. Am. Chem. Soc.* **2005**, *127*, 2398–2399.
- Zhang, J. M.; Zhang, S. J.; Dong, K.; Zhang, Y. Q.; Shen, Y. Q.; Lv, X. M. *Chem.—Eur. J.* **2006**, *12*, 4021–4026.
- Kagimoto, J.; Fukumoto, K.; Ohno, H. *Chem. Commun.* **2006**, *21*, 2254–2256.
- Fukumoto, K.; Ohno, H. *Chem. Commun.* **2006**, *29*, 3081–3083.
- Rochelle, G. T. *Science* **2009**, *325*, 1652–1654.
- Wang, X.; Akhmedov, N. G.; Duan, Y.; Luebke, D.; Li, B. *J. Mater. Chem. A* **2013**, *1*, 2978–2982.
- Gray, M.; Hoffman, J.; Hreha, D.; Fauth, D.; Hedges, S.; Champagne, K.; Pennline, H. *Energy Fuels* **2009**, *23*, 4840–4844.
- Jiang, B.; Kish, V.; Fauth, D. J.; Gray, M. L.; Pennline, H. W.; Li, B. *Int. J. Greenhouse Gas Control* **2011**, *5*, 1170–1175.
- Zhang, Z.; Wu, L.; Dong, J.; Li, B. G.; Zhu, S. *Ind. Eng. Chem. Res.* **2009**, *48*, 2142–2148.
- Li, B.; Jiang, B.; Fauth, D. J.; Gray, M. M. L.; Pennline, H. W.; Richards, G. A. *Chem. Commun.* **2011**, *47*, 1719–1721.
- Crosthwaite, J. M.; Muldoon, M. J.; Dixon, J. K.; Anderson, J. L.; Brennecke, J. F. *J. Chem. Thermodyn.* **2005**, *37*, 559–568.
- Fredlake, C. P.; Crosthwaite, J. M.; Hert, D. G.; Aki, S. N. V. K.; Brennecke, J. F. *J. Chem. Eng. Data* **2004**, *49*, 954–964.
- Wang, X.; Ding, B.; Yu, J.; Wang, M. R. *Nano Today* **2011**, *6*, 510–530.

- (41) Wang, X.; Ding, B.; Yu, J.; Wang, M.; Pan, F. *Nanotechnology* **2010**, *21*, 055502.
- (42) Goepfert, A.; Czaun, M.; May, R. B.; Prakash, G. K. S.; Olah, G. A.; Narayanan, S. R. *J. Am. Chem. Soc.* **2011**, *133*, 20164–20167.
- (43) Khatri, R. A.; Chuang, S. S. C.; Soong, Y.; Gray, M. M. *Energy Fuels* **2006**, *20*, 1514–1520.
- (44) Hwang, C. C.; Jin, Z.; Lu, W.; Sun, Z. Z.; Alemany, L. B.; Lomeda, J. R.; Tour, J. M. *ACS Appl. Mater. Interfaces* **2011**, *3*, 4782–4786.
- (45) Wang, H. B.; Jessop, P. G.; Liu, G. *ACS Macro Lett* **2012**, *1*, 944–948.
- (46) Duan, Y.; Pfeiffer, H.; Li, B.; Romero-Ibarra, I. C.; Sorescu, D. C.; Luebke, D. R.; Halley, J. W. *Phys. Chem. Chem. Phys.* **2013**, *15*, 13538–13558.
- (47) Upadhyay, S. K. *Chemical Kinetics and Reaction Dynamics*; Springer: New York, 2006.
- (48) Jiang, B.; Wang, X.; Gray, M. L.; Duan, Y.; Luebke, D.; Li, B. *Appl. Energy* **2013**, *109*, 112–118.
- (49) Zhao, W. Y.; Zhang, Z.; Li, Z. S.; Cai, N. S. *Ind. Eng. Chem. Res.* **2013**, *52*, 2084–2093.